第 34 卷第 7 期
2018 年 7 月

无 机 化 学 学 报
CHINESE JOURNAL OF INORGANIC CHEMISTRY

Vol.34 No.7
1221-1230

生物活性配体喹啉-2-羧酸根锰(Ⅱ)配位聚合物的晶体结构及生物活性

王仁舒*,[1] 冯 静[1] 雷以柱[1] 杨 丹[1] 朱明昌[2] 邢家领[2] 连明磊[1]

([1]六盘水师范学院化学与材料工程学院,六盘水 553004)

([2]沈阳化工大学配位化学研究室,辽宁省无机分子基化学重点实验室,沈阳 110142)

摘要:合成了一个喹啉-2-羧酸根锰配位聚合物$\{[Mn(Qina)_2(Bpp)]\cdot 2/3H_2O\}_n$,(Qina=2-quinolinecarboxylic-carboxylate,Bpp=4,4′-trimethylenedipyridine)并制得其单晶。运用元素分析、红外光谱和 X 射线单晶衍射等方式表征了配合物结构。晶体结构分析表明,每一个 Mn(Ⅱ)被 2 个 Qina 分子螯合并通过 Bpp 配体桥联而形成一维线性结构;一维分子链通过分子链间的 C–H…π 及 π…π 作用构筑得配合物三维超分子结构。分别利用溴化乙锭荧光光谱法、琼脂糖凝胶电泳法研究了配合物对小牛胸腺 DNA 及质粒 DNA 的结合活性及切割活性。配合物表现出了一定的 DNA 结合力与切割活性。并利用 MMT 比色法,测试了配合物对 Hela,MCF-7 肿瘤细胞株的体外毒性,配合物表现出了一定的体外细胞毒性。

关键词:锰(Ⅱ);配位聚合物;晶体结构;Hirshfeld 表面分析;抗肿瘤活性

中图分类号:O614.71+1 **文献标识码**:A **文章编号**:1001-4861(2018)07-1221-10

DOI:10.11862/CJIC.2018.139

Crystal Structure and Bioactivities of Mn(Ⅱ) Coordination Polymer with Biological Ligand of 2-Quinolinecarboxylic-carboxylate

WANG Ren-Shu*,[1] FENG Jing[1] LEI Yi-Zhu[1] YANG Dang[1]

ZHU Ming-Chang[2] XING Jia-Ling[2] LIAN Ming-Lei[1]

([1]*School of Chemistry and Materials Engineering, Liupanshui Normal University, Liupanshui, Guizhou* 553004, *China*)

([2]*Key Laboratory of the Inorganic Molecule-Based Chemistry of Liaoning Province and Laboratory of Coordination Chemistry, Shenyang University of Chemical Technology, Shenyang* 110142, *China*)

Abstract: A coordination polymer of $\{[Mn(Qina)_2(Bpp)]\cdot 2/3H_2O\}_n$ (Qina=2-quinolinecarboxylic-carboxylate, Bpp=4,4′-trimethylenedipyridine) was synthesized and successfully obtained as single crystals. In the crystal, each Mn(Ⅱ) ion is chelated by two Qina groups, with each Bpp ligand bridging two Mn(Ⅱ) ions to form the 1D polymer chains. Furthermore, the 3D supramolecular architecture is directed by 1D-interchains via weak stacking interactions of C–H…π and π…π. The competition capacity of the complex about calf thymus DNA (ct-DNA) was also analyzed by fluorescence spectroscopy. The ability of complex to cleave the plasmid DNA (pBR322-DNA) was determined by gel electrophoresis assay. And the cytotoxic activity of complex was reviewed for two kinds of cancer cell lines (Hela, MCF-7), which results show that the coordination polymer has *in vitro* anti-tumor activity and cytotoxicity. CCDC: 1550803.

Keywords: Mn(Ⅱ); coordination polymer; crystal structure; Hirshfeld surface analysis; antitumor activity

收稿日期:2017-12-22。收修改稿日期:2018-03-28。

国家自然科学基金(No.21763017),贵州省科学技术厅、六盘水市科学技术局、六盘水师范学院联合科技基金(黔科合 J 字 LKLS[2013]20 号,[2014]7450 号),贵州省教育厅青年科技人才成长项目(黔教合 KY 字[2017]271 号)资助。

*通信联系人。E-mail:wangrenshu@126.com

0 Introduction

Owing to their wide and potential applications in the fields of adsorption, catalysis, magnetism, luminescent, anti-cancer activity, and so on, great attention has been drawn to metal-organic coordination polymers[1-5]. These extended coordination polymers have molecular topological structures, which are mainly based on *N*,*N*-bidentate bridging ligands such as 1,2-bis (2-pyridyl)ethylene and 4,4′-trimethylenedipyridine[6]. Heteroaromatic *N*,*N*-bidentateligands is a kind of molecule with rigid structure[7], which means the effects of $\pi\cdots\pi$ and $C-H\cdots\pi$ are involved in the synthesis of the coordination polymers[8]. More recently, attractive forces of $\pi\cdots\pi$ and $C-H\cdots\pi$ effect have been proved to play significant roles in a variety of biological phenomena[9-10]. On the other hand, the flexible structure that connected with the nitrogen-containing heterocyclic of the aliphatic chain owns various lengths, which means, the carbon chain of the N,N-bidentate ligands exhibit various efficiencies in DNA-binding rate for DNA of biological cell and the cytotoxic activity[11].

N-O chelate ligands are widely-used and strong chelating agents coordinated to transition metal cations. 2-Quinolinecarboxylic acid, has three potential coordination sites, including two oxygens of carboxylate groups and one pyridinic nitrogen[12-13]. Meanwhile, as the quinaldic acid is a bioactive molecule in regard for the metabolism of tryptophan, it should be conducive to applications in pharmaceutical[14].

Conventional small molecule of metal-based anticancer drugs applied to clinical trials, such as species Ru(Ⅲ) complexes are restricted for demerits of general toxicity and drug resistance [15-17]. Due to their small sizes, small molecule complexes cannot accumulate efficient enough at tumor sites. Similarly, the complexes may get lost rapidly from the blood stream due to their poor biocompatible[18].

As an ingredient of glycosyltransferase and phosphoenolpyruvate carboxylase, manganese is necessary for human beings[19-21]. Additionally, some special Mn(Ⅱ) complexes could imitate as catalase, to decrease the transporting channels with ATP-related Ca^{2+} under certain conditions. Thus special Mn(Ⅱ) complexes can induce the apoptosis of tumour cells[22-24].

Consequently, the researchers have focused on developing low-toxic anti tumor agents, thus the metal complexes cultivated by constituents of Mn(Ⅱ), 2-quinolinecarboxylic acid and 4,4′-trimethylenedipyridine are selected. In this paper, the synthesis and characterization of the coordinator polymer $\{[Mn(Qina)_2(Bpp)]\cdot 2/3H_2O\}_n$ will be presented specifically, as well as the evaluation for ct-DNA-binding abilities by using fluorescence spectroscopy. Its cleavage behavior toward pBR322-DNA and cytotoxicity of HeLa and MCF-7 *in vitro* will also be investigated.

1 Experimental

1.1 Materials and instruments

All reagents are purchased through commercial channels and directly used without any treatment. As for analysis, a model Finnigan EA 1112 is employed for Elemental analyses (including C, H and N); and a Thermo Nicolet 380 FT-IR spectrophotometer for IR analysis by KBr disks method. And simultaneous thermogravimetry-differential scanning calorimetry (TG-DSC) was measured on a NETZSCH STA 449 F5 instrument under a dynamic argon atmosphere, and the sample was heated from room temperature to 600 ℃ at a heating rate of 10 ℃·min^{-1}. As well as a Perkin-Elmer LS55 fluorescence spectrofluorimeter for emission spectrum and a JS-380A gel electrophoresis spectrometer for gel electrophoresis.

1.2 Synthesis of $\{[Mn(Qina)_2(Bpp)]\cdot 2/3H_2O\}_n$

For all reagents, the concentration was prepared as 15 mmol·L^{-1}. Firstly, an ethanol-water mixtures (1∶1, *V*/*V*, 10 mL) containing 1.5 mmol of 2-quinolinecarboxylic acid was added into 10 mL of aqueous solution containing 1.5 mmol of $MnCl_2$ dropwise under stirring. After reacting for 6 h at room temperature, another 10 mL of mixture prepared by 1.5 mmol of 4,4′-trimethylenedipyridineand ethanol-water mixtures (1∶1, *V*/*V*) was added and continued the reaction for another 10 h. Subsequently, the pH value of the mixture was adjusted to 8.37 using KOH aqueous

solution to generate yellowish-brown sediment after filtration, and then the sediment was dissolved with acetonitrile-water mixtures (1∶1, *V*/*V*) and stored in the open air. A few days later, the desired yellow transparent crystals were generated and then sequentially filtered and rinsed with water. Anal. Calcd. for $C_{33}H_{25}N_4O_4Mn \cdot 2/3H_2O$ (%):C 65.13, H 5.48, N 9.21; Found(%): C 63.61, H 4.79, N 9.76. IR (KBr, cm^{-1}): 3 237(m), 3 080(w), 2 925(w), 1 708(s), 1 601(m), 1 571 (m), 1 405(m), 1 372(m), 1 213(m), 805(m), 520(w).

1.3 Single crystal X-ray crystallography

The single-crystal X-ray diffraction analysis for complex was conducted by a Bruker SMART APEX2 CCD diffractometer with Mo $K\alpha$ irradiation source (λ= 0.071 073 nm) at 296 K, and intensity data were collected within 2θ range of 3.786°~50.842° by a ω scan technique. Data indexing, integration and absorption correction were done with APEX 2 software package. Structure solution and refinement were done by using SHELXL-2014 software[25-26]. There is an alert level B because the unordered object water molecules are unable to be added the hydrogen atoms. To facilitate the analysis of crystal structure, the highly disordered solvent molecules in the structure were squeezed and refined by used the PLATON and the SHELXL. All non-hydrogen atoms of complex were determined by successive difference Fourier syntheses and refined by full-matrix least squares on F^2. It is found that the locations of all hydrogen atoms are theoretically correct. Selected crystal data of the complex is listed in Table 1.

CCDC: 1550803.

Table 1　Crystal data and structure refinement for the complex

Formula weight	608.51	*F*(000)	1 256
Crystal system	Monoclinic	Crystal size / mm	0.22×0.2×0.18
Space group	$P2_1/n$	Index ranges	$-15 \leqslant h \leqslant 15, -16 \leqslant k \leqslant 16, -19 \leqslant l \leqslant 0$
a / nm	1.338 030(10)	Reflection collected	10 586
b / nm	1.413 840(10)	Independent reflection	5 461(R_{int}=0.046 2)
c / nm	1.619 370(10)	Data, restraint, parameter	5 461, 4, 379
β / (°)	95.159 0(10)	Goodness-of-fit on F^2	0.908
Volume / nm^3	3.051 05(4)	Final *R* indexes [$I \geqslant 2\sigma(I)$]	R_1=0.076 8, wR_2=0.215 2
Z	1	Final *R* indexes (all data)	R_1=0.125 7, wR_2=0.244 3
D_c / ($g \cdot cm^{-3}$)	1.325	Largest diff. peak and hole / ($e \cdot nm^{-3}$)	0.925 and −425
μ / mm^{-1}	0.478		

1.4 Hirshfeld surface calculations

The analytical cif file of the complex molecule was carried out by the CrystalExplorer software[27]. And all the Hirshfeld surfaces were output at the highest resolution. Moreover, the translated command whose coordinate range is from 0.08 to 0.3 nm was selected. And it was applied to all the fingerprint plots.

1.5 Fluorescence spectrum

The molecule of ethidium bromide (EtBr) for fluorophore labeling, has a conjugate planar, the fluorescence intensity of which is extremely weak. But fluorescence intensity is significantly increased if EtBr is specifically intercalated among the base pairs of double strands. The effects of complex difference in concentration are competitive binding with DNA-ethidium bromide (c_{DNA}=5.0 μmol·L^{-1}, c_{EtBr}=1 μmol·L^{-1}, $c_{complex}/c_{DNA}$=1.0, 2.0, 3.0, 4.0). The buffer of 50 mmol·L^{-1} Tris-HCl, pH 7.4, which contains 10 mmol·L^{-1} NaCl, was used in the binding studies. The sample was firstly incubated at temperature of 20 ℃ for 4 h before spectral analysis[28]. The excitation wavelength for fluorescence measurement was 615 nm, while the emission range was set in scope of 550 and 750 nm.

1.6 Gel electrophoresis experiments

As regards to the gel electrophoresis experiments, the pBR322 DNA (0.33 mg·mL^{-1}) was mixed with the complex and then the mixture was incubated at room temperature for 1.5 h. The samples were electrophoresed at 90 V for 1.5 h on 0.8% agarose gel in Tris-acetate buffer (50 mmol·L^{-1} Tris-acetate, 18

mmol·L^{-1} NaCl buffer, pH=7.4). Finally, the gels were stained with 1.0 mg·mL^{-1} EtBr and then photographed under UV light[29].

1.7 Cytotoxicity assay

The MTT assay was used to evaluate the growth inhibitory effect of metal complex on the HeLa and MCF-7 cells. Briefly, cells cultured in RPMI-1640 containing 10% fetal bovine serum, was placed in 37 ℃ and 5% CO_2 incubator. The 96-well culture plate was accurately inoculated with 3×10^4 cells suspension in 100 μL and then incubated for 24 h. RPMI-1640 was used to dilute the solution of complex and 150 μL solution was joined to each well. Besides, the highest concentration of DMSO concentration was not higher than 0.1% and each concentration was under three replication settings. After 72 h, the old solution was cleaned by using 200 μL of saline for each well. MTT solution was diluted for 10 times with RPIM1640. In addition, 100 μL of MTT solution (0.5 mg·mL^{-1}) was added into each well and then was cultivated for 3 h. Subsequently, the media containing MTT was removed, and the formazan crystals were dissolved with 150 μL of DMSO under ambient temperature for 0.5 h. The absorbance value of each hole was measured respectively at 492 and 630 nm[30]. However, the effects of the cisplatin on cell growth were studied in another experiment which was treated as a control team.

2 Results and discussion

2.1 Crystal structure determination

Results of single-crystal X-ray analyses indicated that complex was monoclinic system with $P2_1/n$ space group. The single crystal X-ray diffraction analysis showed that each manganese(Ⅱ) ion is six-coordinated by two nitrogen atoms originated from two molecules of 4,4′-trimethylenedipyridine, as well as two oxygen atoms and two nitrogen atoms that separately from two respective quinoline-2 carboxylic acid ligands (N1-O2, N2-O3). The base structure of polymer complex is shown in Fig.1, and the chosen bond lengths and bond angles are tabulated as Table 2. Besides, along *c* axis,

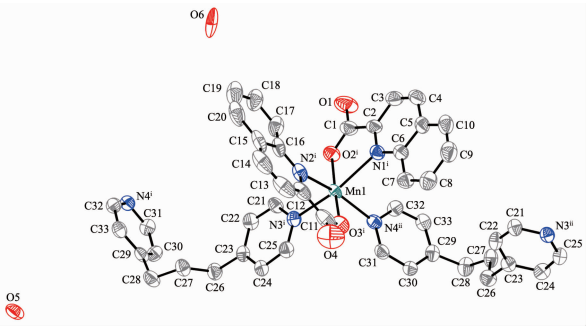

H atoms were omitted for clarity; displacement ellipsoids are drawn at the 30% probability level; Symmetry codes: [i] −1/2+*x*, 1/2−*y*, 1/2+*z*; [ii] 1/2+*x*, 1/2−*y*, −1/2+*z*

Fig.1 Structure of the complex

Table 2 Selected bond lengths (nm) and angels (°)

Mn1-N1	0.237 2(3)	Mn1-N4^{i}	0.227 0(2)	N4-Mn1^{ii}	0.227 0(2)
Mn1-N2	0.237 0(3)	Mn1-O2	0.211 4(2)		
Mn1-N3	0.226 1(3)	Mn1-O3	0.211 3(2)		
N2-Mn1-N1	94.32(9)	O3-Mn1-N1	101.97(10)	C16-N2-Mn1	130.9(2)
N3-Mn1-N1	163.32(10)	O3-Mn1-N2	73.23(10)	C21-N3-Mn1	121.1(2)
N3-Mn1-N2	91.79(9)	O3-Mn1-N3	94.65(9)	C25-N3-C21	116.6(3)
N3-Mn1-N4^{i}	92.40(9)	O3-Mn1-N4^{i}	86.05(9)	C25-N3-Mn1	122.2(2)
N41-Mn1-N1	87.39(8)	O3-Mn1-O2	174.17(9)	C31-N4-C32	115.4(3)
N41-Mn1-N2	159.12(10)	C2-N1-C6	118.4(3)	C31-N4-Mn1^{ii}	122.6(2)
O2-Mn1-N1	73.41(9)	C2-N1-Mn1	110.3(2)	C32-N4-Mn1^{ii}	120.8(2)
O2-Mn1-N2	103.27(10)	C6-N1-Mn1	131.1(2)	C1-O2-Mn1	122.4(2)
O2-Mn1-N3	90.09(9)	C12-N2-C16	118.4(3)	C11-O3-Mn1	121.9(3)
O2-Mn1-N4^{i}	97.17(9)	C12-N2-Mn1	110.6(3)		

Symmetry codes: [i] −1/2+*x*, 1/2−*y*, 1/2+*z*; [ii] 1/2+*x*, 1/2−*y*, −1/2+*z*

the fragments of [Mn(Qina)$_2$] formed from centric Mn(Ⅱ) ions were in turn bridged by Bpp nitrogen atoms, resulting in a 1D chain, as shown in Fig.2.

Additionally, stacking interactions of C–H⋯π and π⋯π between the two one-dimension chains was found in the complex. The H30 from pyridine ring of Bpp molecule, will produce the stacking interactions of C–H⋯π by an aromatic ring from Qina in the different chain. The distances between H30 from the Bpp molecule and the benzene ring of the Qina molecule are 0.371 9 nm, which is shorter than the general one of 0.38 nm that was observed in intermolecular C–H⋯π interactions[31], as shown in Fig.3a. Meanwhile, the H20 from benzene ring of Qina

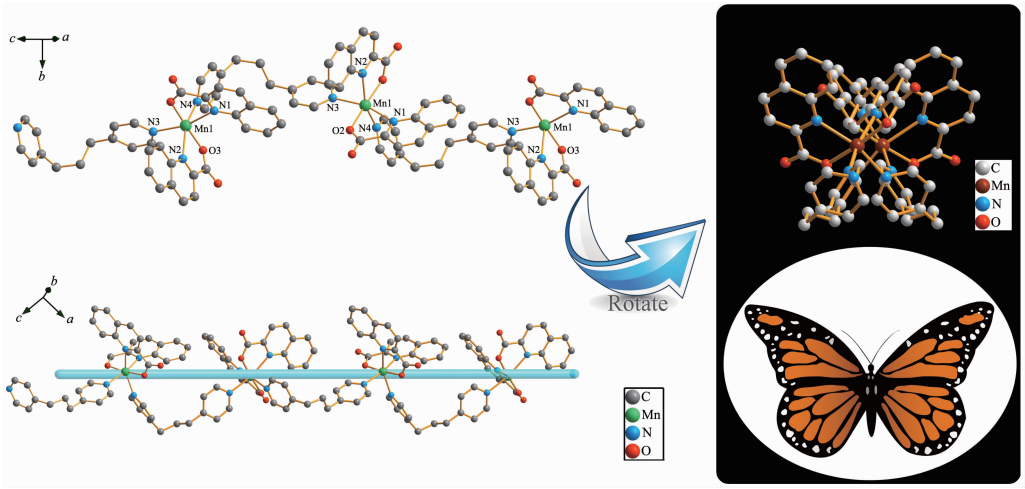

H atoms were omitted for clarity

Fig.2　One dimensional polymeric chain of coordination polymer

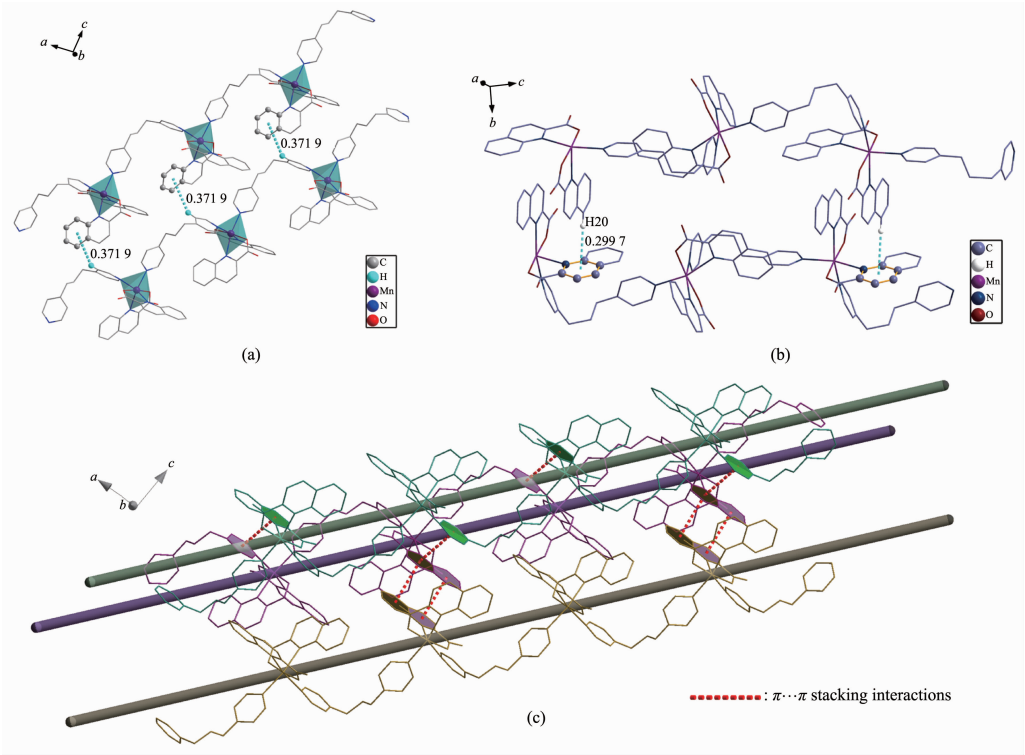

Fig.3　C–H⋯π and π⋯π stacking interactions in the complex: (a) C–H⋯π stacking interactions between Bpp molecule and Qina molecule; (b) C–H⋯π stacking interactions between two Qina molecules; (c) π⋯π stacking interactions between multiple 1D molecular chains

molecule, will also produce the stacking interactions of C–H···π by a pyridine ring from Qina in the different chain, as shown in Fig.3b. The centroid-to-centroid distance between a pair of Qina ligands and Bpp ligands possessing $\pi \cdots \pi$ stacking interactions is 0.363 0 and 0.379 6 nm, respectively, which is also within normal ranges[32], as shown in Fig.3c. Finally, the 3D supramolecular architecture is directed by 1D-interchains via weak stacking interactions of C–H···π and π···π (Fig.4).

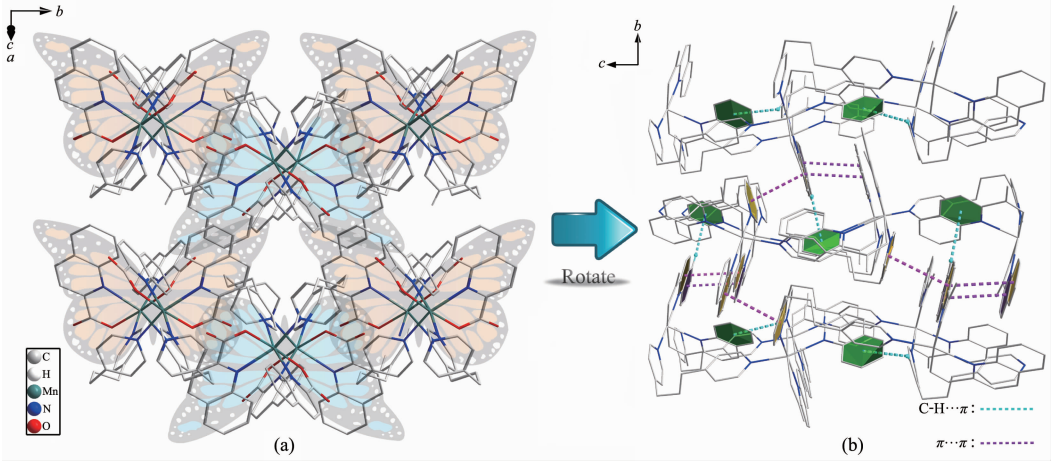

Fig.4 Three dimensional structure of coordination polymer: (a) 3D structure is composed by multiple 1D chains; (b) weak effect superimposed in the supramolecular structure

2.2 Hirshfeld surface analysis

Hirshfeld surface is a way to analyze the intermolecular interactions in a crystal[33]. As shown in Fig.5, there is Hirshfeld d_{norm} surfaces, shape index and curvedness of complex. The red spots or regions on the 3D Hirshfeld surfaces indicate the close-contact interactions, the blue regions represent longer contacts, and the white and green regions represent the distance of contacts. In order to illustrate the weak forces in the crystal better, there are two different observation directions in each type of analysis diagram.

The red parts of the d_{norm} surfaces diagram represents strong intermolecular interactions which represent the C–H···π and $\pi \cdots \pi$ interactions. The red concave with the corresponding positions in shape index and the blue convex of the surrounding receptors complement each other, which has confirmed the existence of such effects[34]. In addition, the white part of the d_{norm} surfaces diagram represents the weak intermolecular interaction which represents the H···H interactions[35]. The curvedness diagram also

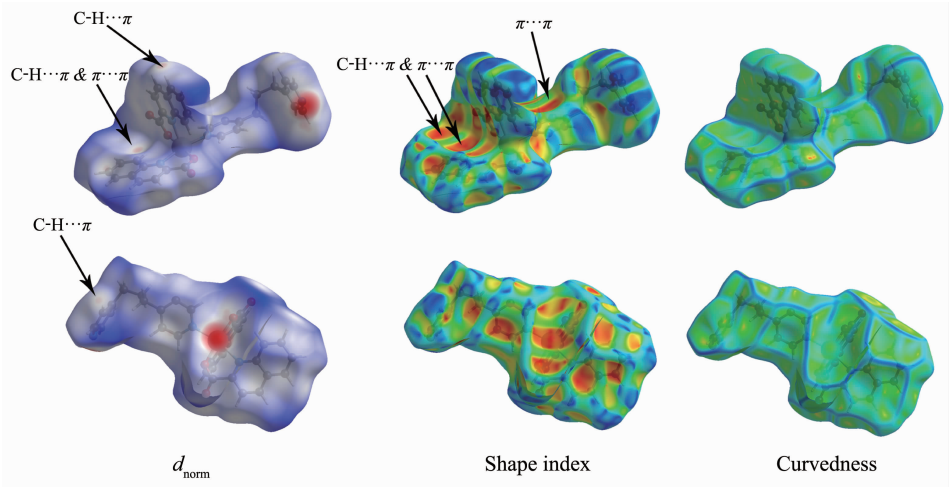

Fig.5 Hirshfeld surface of the complex

shows the same information expressed in the previous two graphs.

Furthermore, the quantitative relationship between the intermolecular interactions of the crystals has also been measured by the 2D fingerprint plots of the CrystalExplorer program. As shown in Fig.6, H⋯H interactions account for the largest proportion of the 2D fingerprint plots. Additionally, the C⋯H interactions are shown on the finger print to represent the symmetrical wing shape, which illustrate that the main intermolecular force between the complex is the C–H⋯π interactions. Moreover, the C⋯C interactions are the evidences that there are weak $\pi\cdots\pi$ effects in the intermolecular of the crystal[36-37]. Besides, it can be obtained from the fingerprint plots that the N⋯H interaction comprises 2.1%, and H⋯O comprises 7.9% of total Hirshfeld surfaces. All Hirshfeld analysis was consistent with single crystal structure analysis.

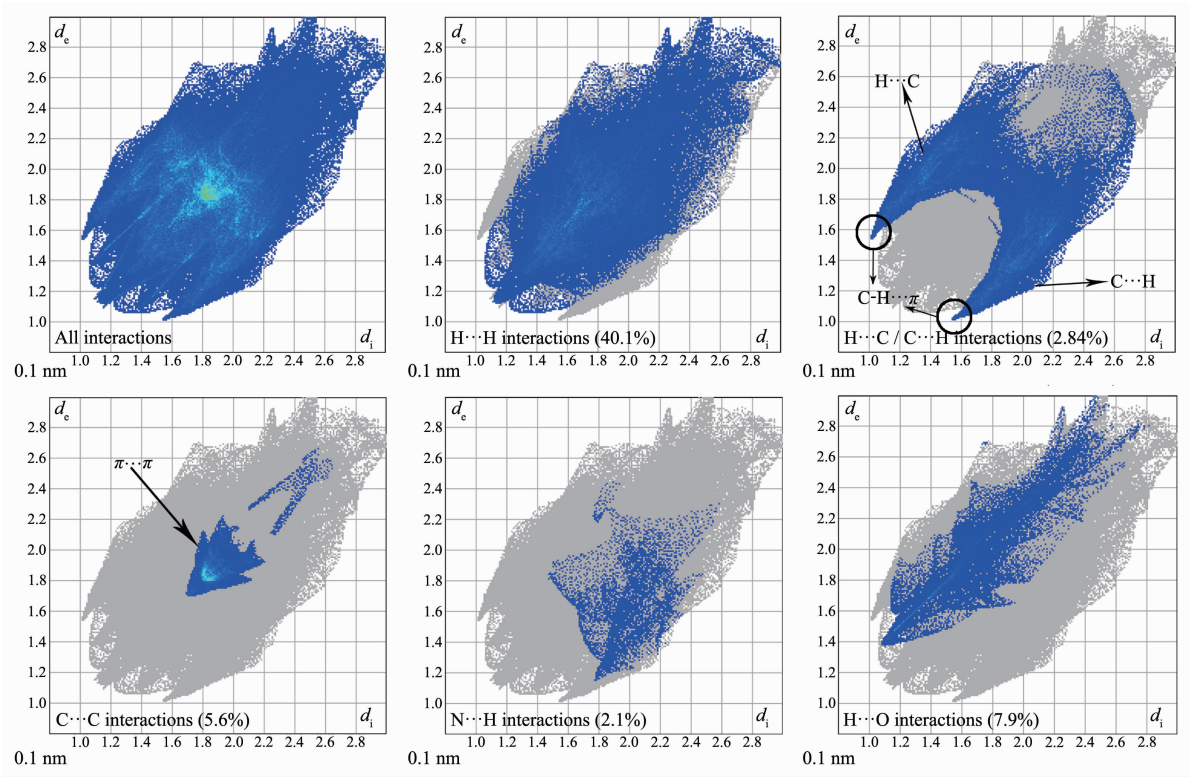

Fig.6　Two dimensional fingerprint plots of the complex

2.3　Thermogravimetric analysis

As shown in the thermogravimetric analysis curve (Fig.7), the complex exhibits three steps of weight losses. The first weight loss corresponding to the removal of lattice solvent is 4.54%　(Calcd. 3.94%) from 190 to 290℃, the second weight loss corresponding to the removal of Bpp ligand is 27.07% (Calcd. 32.58%) from 190 to 300 ℃, and the third weight loss corresponding to the removal of Qina ligand is 52.14% (Calcd. 56.92%) from 300 to 550 ℃.The final formation of the complex is metal oxide MnO (Calcd. 11.66%).

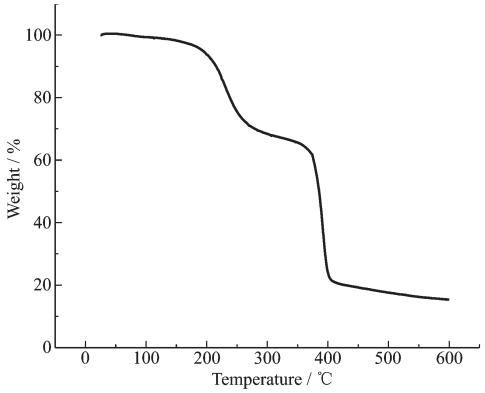

Fig.7　TGA curve of the complex

2.4　Fluorescence spectroscopic properties

Since the complex molecule binds to DNA more strongly than EB, its addition would quench the DNA-induced EB emission[38]. The fluorescence spectra of EB and DNA-bound EB in the absence and presence

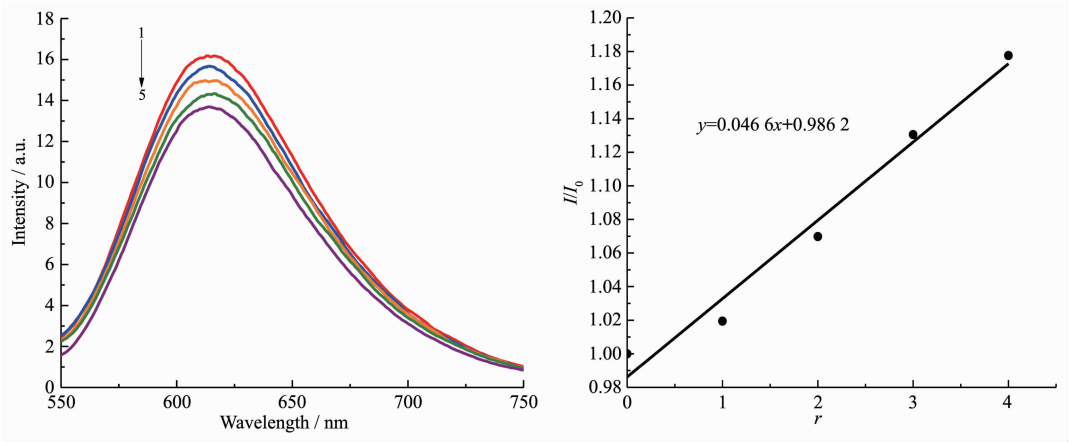

1~5: $r=c_{complex}/c_{DNA}$=0.0, 1.0, 2.0, 3.0, 4.0, respectively

Fig.8 (a) Fluorescence spectra of DNA-EB in the absence and presence of the complex; (b) Stern-Volmer plot for the complex

of the complex is provided as Fig.8.

In the classical Stern-Volmer equation: $I_0/I=1+K_{sq}r$, I_0 and I separately represent the fluorescence intensity with and without the complex; r stands for the total concentration ratio of the complex to that of DNA ($c_{complex}/c_{DNA}$); K_{sq} is the linear Stern-Volmer quenching constant depending on the ratio of the bound concentration of EB to the concentration of DNA, which is generated as the slope of linear curve of I/I_0 against r[39]. The fluorescence quenching curves of DNA-bound EtBr by the complex is also provided in Fig.8. The K_{sq} value for the complex is 0.046 6, which indicates that the complex displaced DNA-bound EB and was bound to DNA with a weak bound at the intercalative mode, due to certain partial weak effect intercalation of the aromatic ring. And the spectrophotometric studies show that the main mode of complex interacting with DNA was electrostatic interaction[40-41].

2.5 Cleavage of extracted pBR322-DNA

The behavior of complex in DNA cleaving was evaluated by monitoring the conversion of the tertiary structure of pBR322 DNA. When circular plasmid DNA is subjected to electrophoresis, the intact supercoiled form (Form Ⅰ) shows a relatively fast migration. While, when scission occurs on one strand of supercoil, it will generate an open circular form (Form Ⅱ)which exhibited a slower-moving migration, and when both strands were cleaved and migrated between Form Ⅰ and Form Ⅱ, it will form a linear form (Form Ⅲ)[42]. The complex can significantly induce the cleavage of the pBR322 DNA at the concentration of 3.23, 6.46 and 12.92 μmol·L^{-1}. As shown in Fig.9, with the increase of concentration of complex, the pBR322 supercoiled DNA (Form Ⅰ) decreases gradually, and the open circular (Form Ⅱ) comes into existence. However, the characteristic of linear (Form Ⅲ) was not obviously changed. The complex has the moderate intensity cleavage of pBR322 DNA, which is in agreement with the trend found in fluorescence quenching experiment.

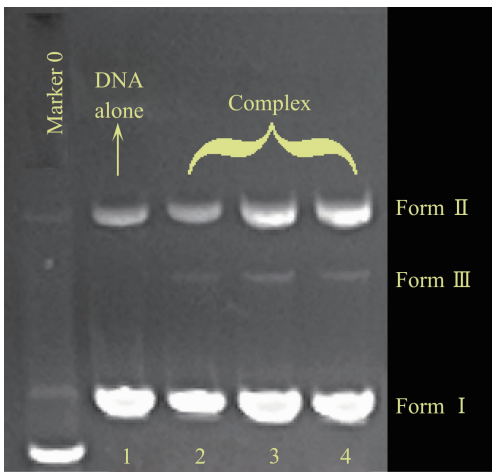

Line 0: Marker; Line 1: DNA alone; Line 2~4: in the different concentrations of the complex: 3.23, 6.46, 12.92 μmol·L^{-1}, respectively

Fig.9 DNA strand break in HeLa cells treated with the complex

2.6 Cytotoxicity *in vitro* study

The prepared complex was measured in term of

the *in vitro* cytotoxic activity by MTT assay. IC_{50} values estimated for two human tumor cell lines of HeLa and MCF-7 are summarized in Table 3. The complex showed a certain level of anti-tumor activity and cytotoxicity[43].

Table 3　Cytotoxicity of the complex against selected human tumor cells after 72 h of incubation

Complex	IC_{50} / (μmol·L^{-1})	
	HeLa	MCF-7
$\{[Mn(Qina)_2(Bpp)]\cdot 2/3H_2O\}_n$	35.17±0.24	30.32±0.25
Cisplatin	9.90±0.23	9.95±0.24

3　Conclusions

A coordination polymer of $\{[Mn(Qina)_2(Bpp)]\cdot 2/3H_2O\}_n$ was synthesized and characterized in aspects of FT-IR spectroscopy, elemental analysis as well as single-crystal X-ray diffraction. The properties of the complex in DNA binding were tested via fluorescence spectra, and results indicated that the complex behaves varied binding affinities in DNA interaction. The cleavage capability of the complex with respect to pBR322 DNA was reviewed by agarose gel electrophoresis, and the results showed that the complex is efficient in DNA cleaving. Through *in vitro* cytotoxicity experiment, it was testified that the complex possesses a level of toxicity to inhibited Hela and MCF-7 cell lines.

References:

[1] Noro S I, Fukuhara K, Kubo K, et al. *Cryst. Growth Des.*, **2011**,**11**:2379-2385

[2] Zhou S B, Wang X F, Du C C, et al. *CrystEngComm*, **2017**, **19**:3124-3137

[3] DENG Qing-Feng(邓青峰), YU Liang-Min(于良民), LI Xia (李霞). *Chinese J. Inorg. Chem.*(无机化学学报), **2017**,**33**(9): 1561-1567

[4] Zhang X, Wang N, Liu P F, et al. *Polyhedron*, **2017**,**129**:149 -156

[5] Etaiw S E H, Amer S A, Bendary M M E. *J. Inorg. Organomet. Polym. Mater.*, **2011**,**21**:662-672

[6] Taleghani S, Mirzaei M, Eshtiagh H H, et al. *Coord. Chem. Rev.*, **2016**,**309**:84-106

[7] Haque A, Ilmi R, Busaidi I J A, et al. *Coord. Chem. Rev.*, **2017**,**350**:320-339

[8] Guo Y, Xu L, Liu H, et al. *Adv. Mater.*, **2015**,**27**:985-1013

[9] Gao E J, Lin L, Zhang Y, et al. *Eur. J. Med. Chem.*, **2011**, **46**:2546-2554

[10]Singh M, Butcher R J, Singh N K. *Polyhedron*, **2009**,**28**:95-100

[11]Gao E J, Zhu M C, Liu L, et al. *Inorg. Chem.*, **2010**,**49**:3261 -3270

[12]Ye J W, Wang Q Q, Gao H Z, et al. *Inorg. Chim. Acta*, **2012**, **384**:1-7

[13]Gao E J, Zhu M C, Zhang W Z, et al. *Russ. J. Coord. Chem.*, **2009**,**35**:621-627

[14]Zhou P, O′Hagan D, Mocek U, et al. *J. Am. Chem. Soc.*, **1989**,**111**:7274-7276

[15]Casolaro M, Cini R, Del B B, et al. *Biomacromolecules*, **2009**,**10**:944-949

[16]Sullivan S T, Ciccarese A, Fanizzi F P, et al. *Inorg. Chem.*, **2009**,**39**:836-842

[17]Caruso F, Rossi M, Benson A, et al. *J. Med. Chem.*, **2012**, **55**:1072-1081

[18]Sun W, Li S, Haupler B, et al. *Adv. Mater.*, **2017**,**29**:1603702

[19]Yang P, Klimistavantzis D J. *Biol. Trace Elem. Res.*, **1998**, **64**:275-288

[20]Miller R S, Mildvan A S, Chang H C, et al. *J. Biol. Chem.*, **1968**,**243**:6030-6040

[21]Rico H, Gómez Raso N, Revilla M, et al. *Eur. J. Obstet. Gynecol. Reprod. Biol.*, **2000**,**90**:97-101

[22]Miguel L L. *Cancer Lett.*, **2007**,**252**:1-8

[23]Zhou D F, Chen Q Y, Qi Y, et al. *Inorg. Chem.*, **2011**,**50**: 6929-6937

[24]Chen Q Y, Zhou D F, Huang J, et al. *J. Inorg. Biochem.*, **2010**,**104**:1141-1147

[25]Sheldrick G M. *Acta Crystallogr. Sect. A*: *Found. Crystallogr.*, **2015**,**A71**:3-8

[26]Sheldrick G M. *Acta Crystallogr. Sect. C*: *Cryst. Struct. Commun.*, **2015**,**C71**:3-8

[27]Liu Q L, Yang L J, Luo Y H, et al. *Res. Chem. Intermed.*, **2016**,**42**:6947-6957

[28]Gao E J, Zhang Y, Lin L, et al. *J. Coord. Chem.*, **2011**,**64**: 3992-4005

[29]Rossiter C S, Mathews R A, Morrow J R. *J. Inorg. Biochem.*, **2009**,**101**:925-934

[30]Hsu C P, Kao T K, Chang W L, et al. *Eur. J. Surg. Oncol.*, **2011**,**37**:140-147

[31]Tsuzuki S. *Annu. Rep. Prog. Chem. Sect. C*: *Phys. Chem.*, **2012**,**108**:69-95

[32]Oszajca M, Nitek W, Rafalska L A, et al. *Cryst. Res. Technol.*, **2015**,**50**:781-790

[33]FENG Chao(冯超), ZHANG Duo(张舵), ZHOU Shi-Yan(周士艳), et al. *Chinese J. Inorg. Chem.*(无机化学学报), **2016**, **32**(7):1215-1222

[34]Seth S K, Sarkar D, Kar T. *CrystEngComm*, **2011**,**13**:4528-4535

[35]Seth S K. *J. Mol. Struct.*, **2014**,**1064**:70-75

[36]Spackman M M, McKinnon J J. *CrystEngComm*, **2002**,**4**:378-392

[37]McKinnon J J, Jayatilaka D, Spackman M A. *Chem. Commun.*, **2007**:3814-3816

[38]Zhu M C, He W X, Gao E J, et al. *Life. Sci.*, **2012**,**90**:519-524

[39]WANG Hui(王慧), GAN Guo-Qing(甘国庆), QU Yang(瞿阳), et al. *Chinese J. Inorg. Chem.*(无机化学学报), **2012**,**28**(6):1217-1221

[40]Satyanarayana S, Dabrowiak J C, Chaires J B. *Biochemistry*, **1993**,**32**:2573-2548

[41]YANG Hao(杨浩). *Chem. J. Chinese Universities*(高等学校化学学报), **2007**,**28**(5):872-876

[42]Rajendiran V, Karthik R, Palaniandavar M, et al. *Inorg. Chem.*, **2007**,**46**:8208-8221

[43]SHI Lei(史蕾), YANG Wen-Cong(杨文聪), ZENG Shu-Ying(曾淑莹), et al. *Chem. J. Chinese Universities*(高等学校化学学报), **2016**,**37**(6):1059-1068